Modeling diffusive dynamics in adaptive resolution simulation of liquid water

Silvina Matysiak and Cecilia Clementi
Department of Chemistry, Rice University, Houston, Texas 77005, USA

Matej Praprotnik,[a] Kurt Kremer, and Luigi Delle Site
Max-Planck-Institut für Polymerforschung, Ackermannweg 10, D-55128 Mainz, Germany

We present a dual-resolution molecular dynamics (MD) simulation of liquid water employing a recently introduced Adaptive Resolution Scheme (AdResS). The spatially adaptive molecular resolution procedure allows for changing from a coarse-grained to an all-atom representation and vice versa on-the-fly. In order to find the most appropriate coarse-grained water model to be employed with AdResS, we first study the accuracy of different coarse-grained water models in reproducing the structural properties of the all-atom system. Typically, coarse-grained molecular models have a higher diffusion constant than the corresponding all-atom models due to the reduction in degrees of freedom (DOFs) upon coarse-graining that eliminates the fluctuating forces associated with those integrated-out molecular DOFs. Here, we introduce the methodology to obtain the same diffusional dynamics across different resolutions. We show that this approach leads to the correct description of the here relevant structural, thermodynamical, and dynamical properties, i.e., radial distribution functions, pressure, temperature, and diffusion, of liquid water at ambient conditions. © *2008 American Institute of Physics.* [DOI: 10.1063/1.2819486]

I. INTRODUCTION

Water is a typical example where the interplay between different length scales determines the relevant properties of the system. Including explicit water in large biomolecular simulations is crucial[1,2] but normally not feasible due to the large number of water molecules needed to describe biomolecular function. The computational requirements of all-atom simulations in explicit water usually do not allow investigation of biologically relevant time scales.[3] Most computational approaches renormalize the role of water into the definition of effective inter-residue interactions[2] or as a continuous field, in order to focus the computational efforts to simulate the biomolecule. However, the discrete nature of water molecules can play a role in, e.g., controlling protein functionality or the case of interactions between hydrocolloids and water, where hydrogen bonding is important, etc. To overcome this problem, a multiscale modeling of water can be very advantageous to speed up the simulation without losing physico-chemical accuracy.

Multiscale modeling is emerging as a viable way to bridge the various length and time scales involved in complex molecular systems.[4–14] In general, to build a multiscale model two main issues need to be addressed. The first issue consists of mapping the system into a robust reduced model while preserving the here relevant physico-chemical properties, i.e., radial distribution functions, pressure, and temperature, of the reference all-atom system. The second issue involves the definition of a robust and physically accurate

procedure to smoothly join the different resolutions. We have recently proposed the Adaptive Resolution Scheme (AdResS) (Refs. 15 and 16) to address both issues for a system of water molecules.[17] Typically, the reduction in the number of the system's degrees of freedom (DOFs) upon coarse-graining introduces a time scale difference between the coarse-grained and explicit region. Although in certain instances the difference in time scale may be advantageous for reaching longer simulation times, in other cases having the correct diffusional dynamics is crucial. This is the case, for instance, if a dynamical property is the focus of an investigation as in the translocation of biopolymers through membrane nanopores.[18]

In this paper, in order to justify our choice of the recently introduced single-site water model[17] as the optimal coarse-grained water model to be used with AdResS (when using the standard three-site TIP3P water model[19] as the all-atom water model), we present first a detailed analysis and comparison of newly developed coarse-grained water models having a different number of DOFs (from 3 to 9) with the single-site water model[17] as well as the TIP3P water model.[19] In this way we can study the contribution of separate DOFs of the all-atom water model to the definition of its structural properties. As it turns out, the single-site water model can reproduce the structural and thermodynamical properties of the all-atom system that are relevant for the multiresolution simulation equally well as the more sophisticated models. Therefore, we have chosen it as the coarse-grained model in our adaptive resolution simulations. Next, we introduce the methodology to obtain the same diffusional dynamics across the different resolutions in the hybrid atomistic/coarse-
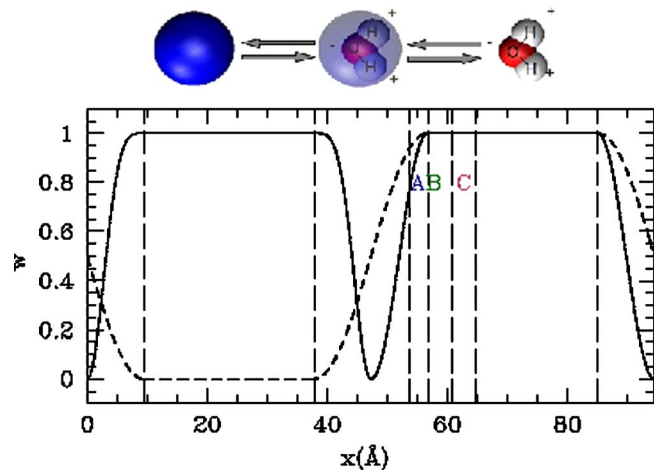

FIG. 1. (Color online) Top figure: The coarse-grained molecule is represented at the left, and the all-atom water molecule is represented at the right. The middle hybrid molecule interpolates between the two. Bottom figure: The dashed line represents the weighting function $w(x) \in [0,1]$ defined in Ref. 15 and discussed in the text. The values $w=1$ and $w=0$ correspond to the atomistic and coarse-grained regions of the hybrid atomistic/mesoscopic system, respectively. The full line represents the interface correction weighting function $s(w)$ defined in Fig. 6. The value $s=1$ corresponds to the atomistic and coarse-grained regions, while $s=0$ when $w=1/2$. The explicit and interface regions are divided into three regions (A,B,C) of width 4 Å for computing the cosine distribution in Fig. 8.

grained (ex-cg) model system composed of explicit and coarse-grained molecules as presented in Fig. 1.

II. MAPPING OF A COARSE-GRAINED MODEL TO THE ALL-ATOM REPRESENTATION

In order to map a coarse-grained to an all-atom model, we have to construct an effective potential between coarse-grained molecules in a way that the atomistic structural properties are reproduced. We numerically build such an effective Hamiltonian following an "inverse statistical-mechanics" approach.[20–22] In order not to bias *a priori* the potential function with the choice of a particular functional form, we introduce a grid approximation, expressing a general pairwise Hamiltonian in the form

$$H = \sum_{\alpha} U_{\alpha} S_{\alpha}, \tag{1}$$

where S_{α} is the number of coarse-grained particles in the interval $\in (r_{\alpha}, r_{\alpha}+dr)$ and U_{α} is the discretized value of the potential in the interval $(r_{\alpha}, r_{\alpha}+dr)$. The averages $\langle S_{\alpha} \rangle$, which can be interpreted as a discretized radial distribution function (rdf), are functions of the set of parameters $\{U_{\alpha}\}$. Values of the potential parameters $\{U_{\alpha}\}$ that reproduce the rdf of the all-atom model can be obtained iteratively as follows:

- The center-of-mass rdf $g(r)$ is computed from all-atom simulations and used as a target function. The potential of mean forces is assumed as an initial approximation to the effective potential function,

$$U_{\alpha}^0 = -kT \ln g(r_{\alpha}), \tag{2}$$

where U_{α} is the potential at a distance r_{α}.

- By comparing the atomistic center-of-mass rdf with the rdf obtained for the coarse-grained model at the nth iteration (with corresponding potential parameters U_{α}^n) the $(n+1)$th correction to the effective potential can be found. Namely, the correction to the potential parameters U_{α}^n is given by the solution of the system of linear equations,[20]

$$\Delta \langle S_{\alpha} \rangle = \sum_{\gamma} \frac{\partial \langle S_{\alpha} \rangle}{\partial U_{\gamma}} \Delta U_{\gamma}, \tag{3}$$

where

$$\frac{\partial \langle S_{\alpha} \rangle}{\partial U_{\gamma}} = -\beta(\langle S_{\alpha} S_{\gamma} \rangle - \langle S_{\alpha} \rangle \langle S_{\gamma} \rangle). \tag{4}$$

- Ensemble averages $\langle S_{\alpha} S_{\gamma} \rangle$ and $\langle S_{\alpha} \rangle$, $\langle S_{\gamma} \rangle$ are computed from MD simulations (with potential parameters U_{α}^n), and the correction ΔU_{α}^n to the potential U_{α}^n is obtained by solving the system of linear equations, Eq. (3),

$$U_{\alpha}^{n+1} = U_{\alpha}^n + \Delta U_{\alpha}^n. \tag{5}$$

- The corrected potential parameters U_{α}^{n+1} are then used to perform molecular dynamics simulation with the coarse-grained model and calculate new ensemble averages for the quantities $\langle S_{\alpha} S_{\gamma} \rangle$ and $\langle S_{\alpha} \rangle$, $\langle S_{\gamma} \rangle$.

The points above are repeated to determine a new set of corrections ΔU_{α}^{n+1}. The procedure is repeated until convergence is reached within the statistical simulation error.

Additionally, to match the pressure of the coarse-grained to the all-atom model, after each iteration a weak constant force is added to the effective force in such a way that the total effective force and potential energy are zero at the fixed cutoff distance r_c,[16,23]

$$\Delta U(r) = U_o \left(1 - \frac{r}{r_c} \right). \tag{6}$$

We use a value of $r_c = 7$ Å as the rdf ≈ 1 for $r > r_c$. Depending on the pressure in the current iteration being above or below the target value corresponding to the pressure of the reference all-atom system, U_o can assume a positive or negative value.

For the atomistic representation of water, we selected the rigid TIP3P model[19] that gives a reasonable description of the behavior of liquid water around standard (physiological) temperature and pressure, and is not too expensive computationally. The potential function of rigid TIP3P involves a rigid water with three interaction sites that coincide with the atomic positions. The model uses atom-centered point charges to represent the electrostatic, i.e., positive charges on the hydrogens and a negative charge on oxygen ($e_O = -2e_H$). The van der Waals interaction between two water molecules is modeled by the Lennard-Jones potential with just a single interaction site per molecule centered on the oxygen atom; the van der Waals interactions involving the hydrogens are omitted. This gives the following potential:
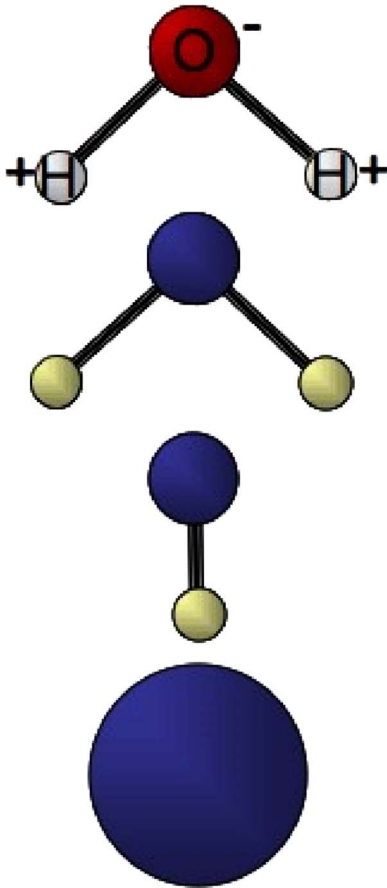
tetrahedral clusters is well below 1 ps in water, atomistic water molecules are not easily united into a coarse-grained bead. The water molecules could move apart in the transition regime of our multiscale model (see Sec. V), which would require redistributing the water molecules into coarse-grained beads on-the-fly. By mapping one atomistic molecule to one coarse-grained molecule, we avoid this problem.

A. Three-site interaction model

A first level of coarse-graining can be introduced by preserving the atomic positions of each atom in the TIP3P water model and replacing the explicit electrostatic interactions [the first term in Eq. (7)] with effective short-ranged interactions. This model preserves explicitly the H-bond directionality but it is computationally less expensive than TIP3P because it removes the long-ranged Coulombic term. The calculated all-atom site-site rdf's are used as input to build the OO, OH, and HH effective potentials [see Eq. (4)]. In order to quantify the agreement of the rdf's (corresponding to the all-atom and coarse-grained model), we introduce the penalty function f_p (Ref. 15) defined as

$$f_p = \int \left[g^{\mathrm{cg}}(r/\sigma_{\mathrm{OO}}) - g^{\mathrm{ex}}(r/\sigma_{\mathrm{OO}}) \right]^2 \exp(-r/\sigma_{\mathrm{OO}}) d(r/\sigma_{\mathrm{OO}}),$$

(8)

where g^{ex} and g^{cg} are the reference site-site rdf of the atomistic and coarse-grained system, respectively, and σ_{OO} is the Lennard-Jones constant of the TIP3P water model.[19] The extremely low values of the f_p obtained (f_p of the OO rdf is 7.9×10^{-5}, for OH is 8.2×10^{-5}, and HH is 1.1×10^{-4}) for the optimized effective potential for the three-site model indicates a perfect matching of the rdf's. The optimized effective potentials are, as expected, very similar to the effective potentials of other previously introduced three-site coarse-grained water models.[28,32] In addition, to check the angular properties (that are not completely defined by the rdf) we computed the distribution of the angle θ formed between the center-of-mass of three nearest-neighbor molecules (Fig. 3, top), and the distribution of the orientational order parameter q (see Fig. 3), as defined by Errington et al.,[33]

$$q = 1 - \frac{3}{8} \sum_{j=1}^{3} \sum_{k=j+1}^{4} \left(\cos \psi_{jk} + \frac{1}{3} \right)^2,$$

(9)

where ψ_{jk} is the angle formed by the lines joining the oxygen atom of a given molecule and those of its nearest neighbors j and k. The parameter q measures the extent to which a molecule and its four nearest neighbors adopt a tetrahedral arrangement. The excellent agreement between the rdf's and the angular distribution suggests that the explicit H-bond directionality is responsible for the local structure. On the contrary, the small deviation of the orientational order parameter distribution suggests that the electrostatic interactions are at least partly responsible for the overall tetrahedral arrangement of the system.

FIG. 2. (Color online) Cartoon of different water models employed in this study. From top to bottom: The rigid TIP3P water model, and three-site, two-site, one-site coarse-grained water models, respectively.

$$H = \sum_i \sum_j \frac{e_i e_j}{r_{ij}} + \frac{A}{r_{\mathrm{OO}}^{12}} - \frac{C}{r_{\mathrm{OO}}^6}.$$

(7)

The values of the parameters e, A, and C are assigned to reproduce reasonable structural and energetics properties of liquid water.[19]

III. COARSE-GRAINED MODELS FOR WATER

Many simplified coarse-grained models have been developed to reproduce the structural properties of water qualitatively.[24] Existing coarse-grained models can of course only reproduce thermodynamical properties of all-atom water to a certain extent.[25–29] By using the procedure described above, we have thus designed water models at different levels of coarse-graining (three-site, two-site, and one-site) schematically depicted in Fig. 2. The gradually increasing level of coarse-graining allows us then to study the contribution of different DOFs to the structural and thermodynamical properties of the reference all-atom system. In this way we can determine the most appropriate coarse-grained model to be used in our adaptive resolution simulations.

An even more efficient way would be if a spherical coarse-grained bead represented several water molecules; see for example Refs. 30 and 31. However, since the lifetime of
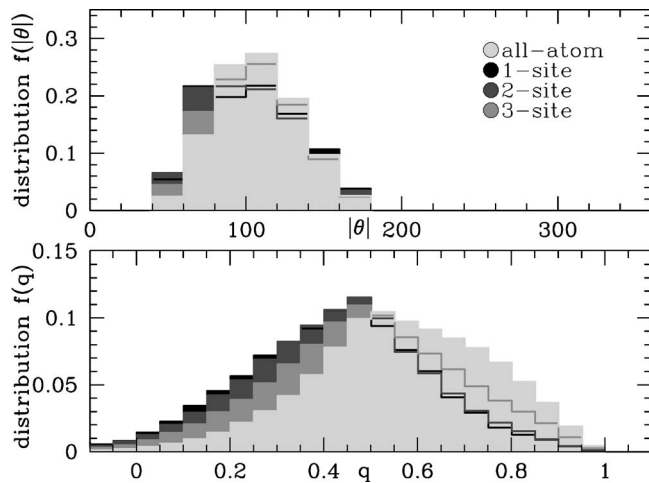
FIG. 3. Top figure: The center-of-mass angular distribution between three nearest neighbors for all-atom, 1-site coarse-grained, 2-site coarse-grained, and 3-site coarse-grained models for water. Bottom figure: The analogous distributions of the orientational order parameter q. The center-of-mass rdf of the different water models coincides exactly with the all-atom rdf (not shown).

B. Two-site interaction model

A two-site simplified model of water changes the symmetry of the molecule by using two interacting sites instead of three, one corresponding to the oxygen atom and the second one providing the directionality of the dipole moment. Since the dipole moment of TIP3P is $\mu = 2.35D$ and the charge separation is $q = 0.82e$,[19] the effective separation of the negative and positive charge centers is $d = \mu/q \approx 0.5966$ Å. Thus, we define the two-site model by representing each water molecule by two spheres, which are joined by a rigid rod of length 0.5966 Å. Two-site models have been previously proposed for water;[26] however, existing models cannot exactly reproduce the radial structure of the reference all-atom water model. The two-site water model with parameters optimized by the procedure described above can reproduce the rdf's remarkably well for the different pairs of interactions: oxygen-oxygen with $f_p = 4.5 \times 10^{-5}$, oxygen-dipole with $f_p = 1.4 \times 10^{-4}$, and dipole-dipole with $f_p = 3.2 \times 10^{-5}$. Figure 3 shows the angular distribution and the orientational order parameter distribution obtained for the two-site model, in comparison with the results of the all-atom and three-site models. The excellent agreement between the rdf's suggests that the inclusion of a dipole center is sufficient for the correct radial structure. The deviation on the angular distribution from the three-site model indicates that the explicit H-bond directionality has a contribution to the angular structure (in addition to the electrostatic contribution, as found in the three-site model).

C. One-site interaction model

In the one-site coarse-grained model, the water is represented by one spherically symmetrical site having a mass $m_O + 2m_H$. As demonstrated in Ref. 17, the one-site model can reproduce the center-of-mass rdf ($f_p = 7.6 \times 10^{-5}$) and thermodynamic properties of the reference all-atom water model with remarkable accuracy. The optimized effective

potential (see the inset of Fig. 5) has a first primary minimum at about 2.8 Å corresponding to the first peak in the center-of-mass rdf. A second, slightly weaker and significantly broader minimum at 4.5 Å corresponds to the second hydration shell. The combined effect of the two leads to local packing close to that of the all-atom TIP3P water. Our effective coarse-grained potential is quite different from the previously suggested potentials:[25–27,34] while in previous one-site models the deepest minimum corresponds to the second hydration shell, the absolute minimum in our model is found in the first shell.

The good structural agreement between the explicit and coarse-grained models indicates that, although our coarse-grained model of water is spherically symmetric and therefore does not have any explicit directionality, it approximately captures the correct local structure. Furthermore, the angular and orientational order parameter distribution coincides with what obtained for the two-site model. Since the one-site model can qualitatively predict the correct angular distribution and is computationally the least expensive of all the coarse-grained models, it was our choice for the multiscale approach (presented in Ref. 17).

As a consequence of the reduced number of DOFs, there is a time scale difference in the dynamics of the coarse-grained system with respect to the atomistic one. The diffusion coefficient increases as the level of coarse-graining is increased, with the diffusion coefficient of the center of mass for the TIP3P model $D \approx 3.7 \times 10^{-5}$ cm²/s, for the three-site model $D \approx 4.68 \times 10^{-5}$ cm²/s, for the two-site model $D \approx 7.54 \times 10^{-5}$ cm²/s, and for the one-site model $D \approx 8.1 \times 10^{-5}$ cm²/s.

Using the one-site coarse-grained model one can significantly speed up the simulation, with a total gain in computational time of a factor $\sim 17 - 20$ when compared to atomistic simulations.[17] This is due to the reduction of the number of interactions, which are also softer than in the atomistic case, and due to an intrinsic time scale difference in the diffusive dynamics of the coarse-grained system, that is faster by about a factor of 2 than the all-atom simulations counterpart (see the above values for the diffusion constant).

IV. MATCHING THE DIFFUSIVE DYNAMICS OF THE COARSE-GRAINED TO THE ALL-ATOM MODEL

As discussed above, the dynamics of the one-site coarse-grained model is faster than that obtained from all-atom simulations. The speed-up occurs because of the reduction in DOFs upon coarse-graining, which eliminates the fluctuating forces associated with those missing molecular DOFs, leading to the much smoother overall energy landscape.[35,36] In our MD simulations we use a Langevin thermostat, and the equations of motion are in the form

$$m_i \frac{dv_i}{dt} = F_i - m_i \Gamma v_i + R_i(t), \tag{10}$$

where $F_i = -(\partial U_i / \partial x_i)$ is the deterministic force and R_i is a stochastic variable with $\langle R_i(t) R_j(t + \tau) \rangle = 2\Gamma m_i kT \delta(\tau) \delta_{ij}$. The coefficient Γ determines the strength of the coupling to the
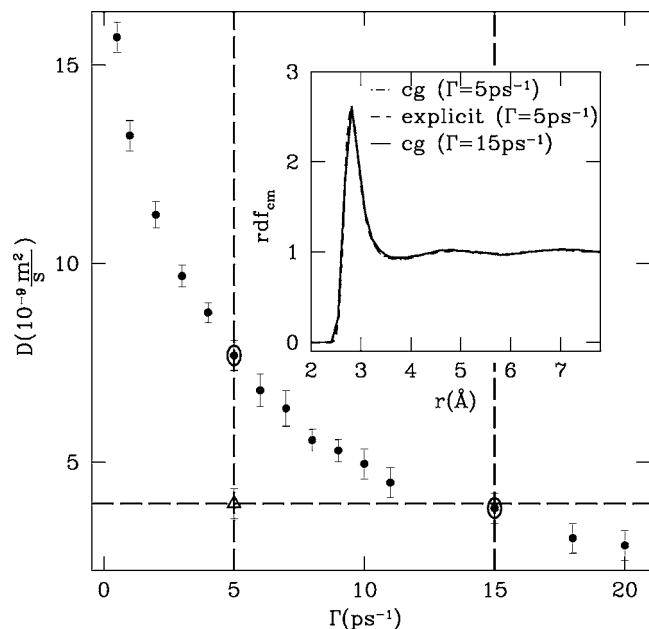
FIG. 4. The diffusion coefficient as a function of the friction constant. The triangle indicates the value obtained for the all-atom diffusion coefficient when a value $\Gamma = 5$ ps^{-1} is used in the simulation. The black dots indicate the diffusion coefficient obtained for the coarse-grained system for different values of Γ. The two circles indicate the diffusion coefficients obtained for the coarse-grained system when $\Gamma = 5$ and $\Gamma = 15$ ps^{-1}, respectively, are used in the simulation. The inset compares the rdf's obtained for the all-atom system and the coarse-grained system for different values of the friction coefficients.

FIG. 5. The center-of-mass rdf's for explicit, ex-cg($w=1/2$), and coarse-grained systems. The inset shows the corrected effective pair potential U_{ic}^{cm} for hybrid molecules [dashed line] and the reference effective potential for the coarse-grained molecules [full line].

bath [not to be confused with the friction coefficient ξ of the system (for TIP3P $\xi = 288.6$ ps^{-1})]. When $1/\Gamma$ is large compared to the typical time scales in the system, the stochastic dynamics reproduces dynamics obtained by molecular dynamics (MD),[37] while if $1/\Gamma$ is small, then the stochastic dynamics deviates significantly from MD. Simulations performed using the one-site model with the same coupling to the bath ($\Gamma = 5$ ps$^{-1} \ll \xi$) that is usually used for TIP3P (Ref. 38) produce an increase of a factor of about 2 in the diffusion time scale of the coarse-grained system. An accelerated dynamics can be advantageous in some cases but, as mentioned previously, it can be a problem if the dynamical properties themselves are under investigation. The coarse-grained dynamics can be slowed down by increasing the effective friction in the coarse-grained system. That is, by changing Γ, the one-site model can mimic the diffusive dynamic of the all-atom system. Figure 4 shows that the diffusion coefficient D monotonically decreases as the coefficient Γ increases. The coarse-grained model yields the same diffusion coefficient as the all-atom system (for which $\Gamma_{ex} = 5$ ps^{-1}) when $\Gamma_{cg} = 15$ ps^{-1}. The additional frictional noise does not affect the short-time dynamics of the system since $\Gamma_{ex} < \Gamma_{cg} \ll \xi$.[37] It is worth mentioning that the structural/thermodynamics of the coarse-grained system are not effected by changes in Γ in this range. Figure 4 shows the perfect agreement between the center-of-mass rdf for the coarse-grained and all-atom system when different values of Γ are used for the two models. However, we have to bear in mind that by employing the Langevin thermostat, Eq. (10), we screen the hydrodynamics. Furthermore, for too large Γ the statistics is also altered
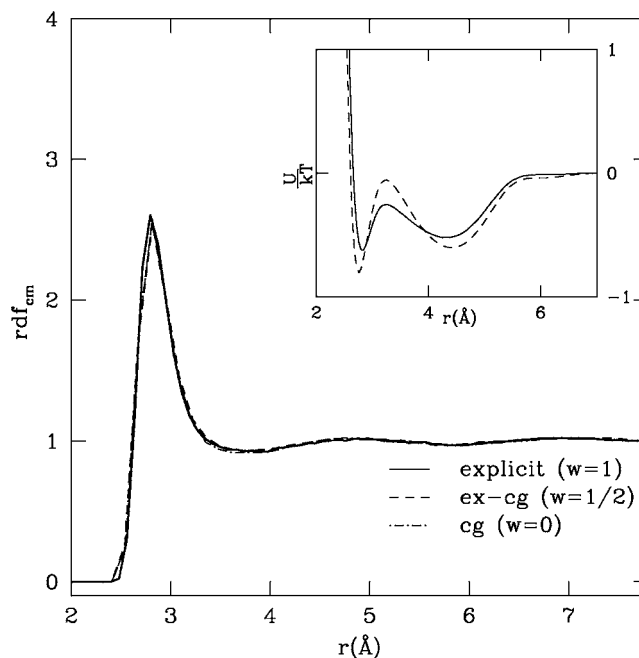
because one arrives eventually at the Brownian dynamics. In order to correctly reproduce the hydrodynamics, one has to resort to the dissipative particle dynamics (DPD) thermostat[39] as was done for instance in Ref. 40 for the case of a macromolecule in the hybrid atomistic/mesoscale solvent.

V. ADAPTIVE RESOLUTION SCHEME (AdResS)

As we have proposed in Ref. 17, we design an adaptive multiscale system where half of the simulation box is occupied by atomistic water molecules and the other half by the corresponding one-site coarse-grained molecules, respectively, as schematically presented in Fig. 1. In order to smoothly couple the regimes of high and low level of detail, we apply the AdResS scheme,[15–17] which allows the molecules to move freely between regimes without feeling any barrier in between. The interface region contains hybrid molecules that are composed of an all-atom molecule with an additional massless center-of-mass particle serving as an interaction site. The transition is governed by a weighting function w that interpolates the molecular interaction forces between the two regimes, and assigns the identity of the molecules. In the present work we used the weighting function defined in Ref. 15 and described in Fig. 1. The function w is defined in such a way that $w=1$ corresponds to the atomistic region, and $w=0$ to the coarse-grained region, whereas the values $0 < w < 1$ correspond to the interface layer. This interpolation leads to intermolecular forces acting on the center-of-mass of the molecules α and β as

$$\mathbf{F}_{\alpha\beta} = w(X_\alpha)w(X_\beta)\mathbf{F}_{\alpha\beta}^{atom} + [1 - w(X_\alpha)w(X_\beta)]\mathbf{F}_{\alpha\beta}^{cm}, \quad (11)$$

where $\mathbf{F}_{\alpha\beta}$ is the total intermolecular force acting between center of mass of molecules α and β. $\mathbf{F}_{\alpha\beta}^{atom}$ is the sum of all
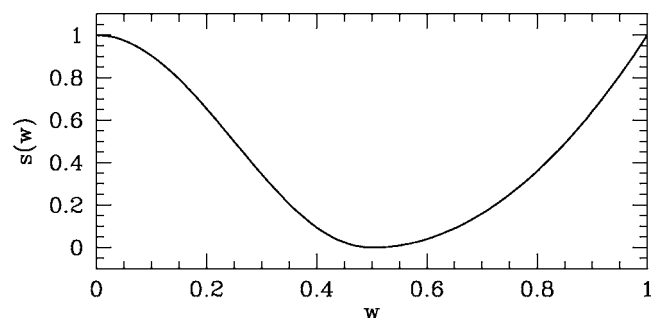
FIG. 6. The interface correction weighting function $s(w)$. The value $s=1$ corresponds to the atomistic and coarse-grained regions and $s=0$ when $w=1/2$.

pair atomic interactions between explicit water atoms of molecule α and explicit water atoms of molecule β, and $\mathbf{F}_{\alpha\beta}^{cm}$ is the effective pair force between the center-of-mass of two water molecules. X_α and X_β are the center-of-mass coordinates of molecules α and β. Note that the AdResS as given by Eq. (11) satisfies Newton's third law. This is crucial for the diffusion of molecules across the resolution boundaries.[14] Since the total force as defined by Eq. (11) depends on the absolute positions of the particles and not only on their relative distances, it is in general not conservative, i.e., the work done by it depends on the path taken in the transition regime. Hence, the corresponding potential does not exist and the total potential energy of the system cannot be defined.[41] Still, the intermolecular forces between molecules outside the transition regime are conservative with well-defined potentials, i.e., the all-atom or effective coarse-grained potentials.[15]

In principle, one could also try to couple the different scales via the respective potentials instead of forces. However, we showed in Refs. 13, 14, and 42 that, although in this
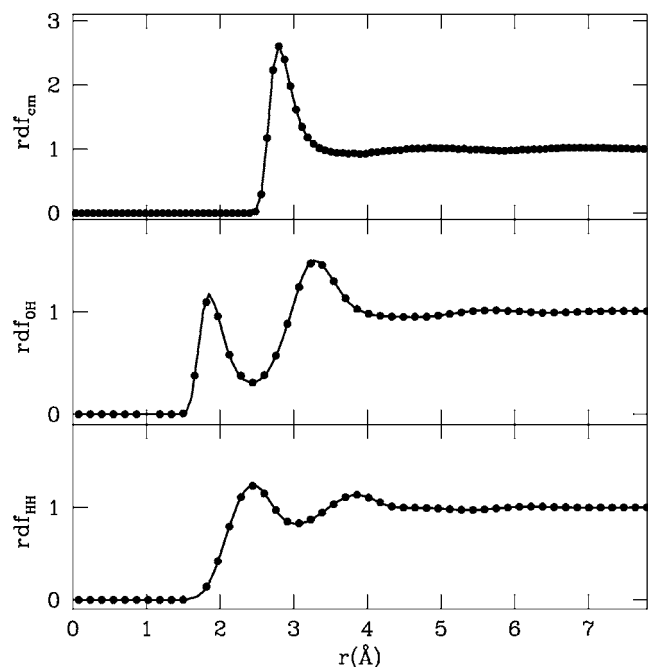

FIG. 7. The center-of-mass (fp=7.65×10^{-5}), OH (fp=6×10^{-5}), and HH (fp=6.6×10^{-5}) rdf's for the explicit region in the hybrid system [dots], and bulk [line] systems.
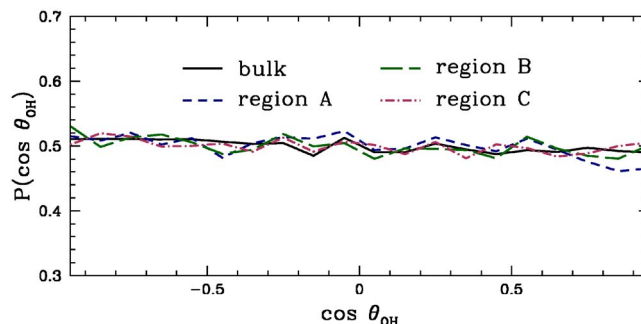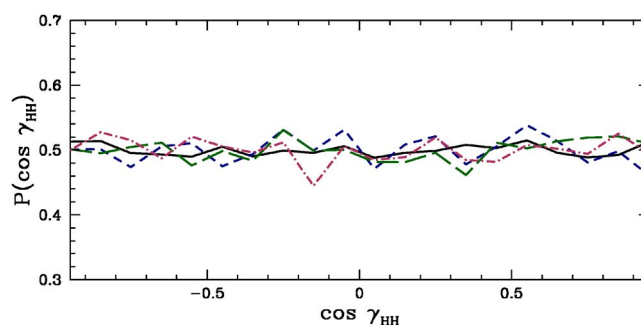

FIG. 8. (Color online) Cosine distribution of the angle formed by the H-H vector (top panel) and O-H vector (bottom panel) of the water molecules with the interface normal vector pointing toward the explicit region in three consecutives regions of width 4 Å each (see Fig. 1 for the definition of the regions).

case the system is conservative with a defined total potential energy, this leads to a violation of Newton's third law and consequently to a nonconservation of the linear momentum. Very recently, an alternative "energy-conserving" approach was proposed in Ref. 43, where the authors proposed a scheme that couples the atomistic and coarse-grained potentials instead of forces. However, the proposed scheme is ultimately the same as AdResS (with a slightly modified weighting function), i.e., Eq. (11) is employed for the force evaluation (satisfying Newton's third law), as the "spurious" forces associated with the potential coupling are neglected. By doing this the computed energies do not correspond to forces employed in integrating the equations of motion.

Each time a molecule crosses the boundary between the different regimes it gains or loses (depending on whether it leaves or enters the coarse-grained region) its equilibrated rotational DOFs while retaining its linear momentum. By this choice of interactions in the interface region, the hybrid molecule interacts with molecules in the coarse-grained region on a coarse-grained level. On the other hand, the interactions of the hybrid molecules with the molecules in the explicit region are a combination of the explicit-explicit and cg-cg interactions to smoothly and efficiently equilibrate additional DOFs upon moving in the explicit regime.[15,16] This change of resolution, which can be thought of in terms of similarity to a phase transition,[13] requires to supply or remove latent heat and thus must be employed together with, i.e., a Langevin thermostat.[15] The thermostat is coupled locally to the particle motion and provides a means to deliver or absorb the latent heat.

As in Ref. 17, the reaction field (RF) method is used, in which all molecules outside a spherical cavity of a
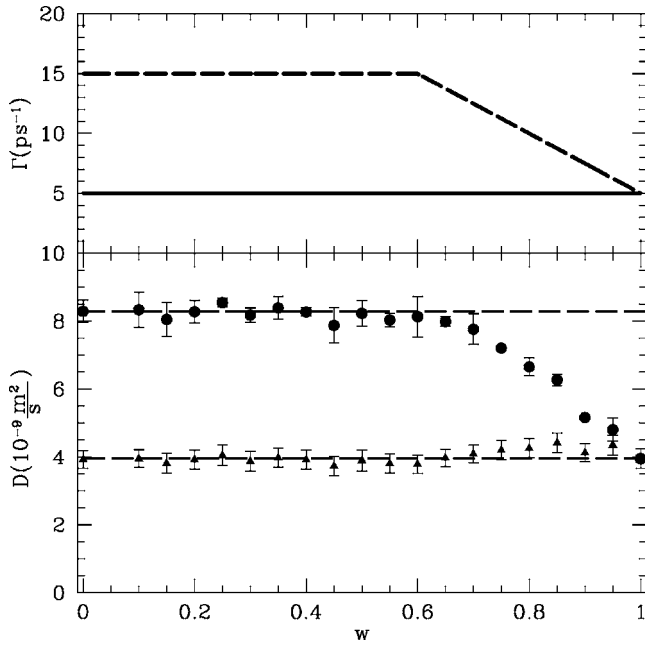
FIG. 9. Top figure: The dashed curve indicates the dependency of the friction coefficient as a function of the particle identity w when a position-dependent thermostat is used. The full line shows the constant value of the friction coefficient when a regular thermostat is used. Bottom figure: The dots indicate the diffusion of the molecules when the regular thermostat is used. The triangles indicate the diffusion of the molecules when the position-dependent thermostat is used.
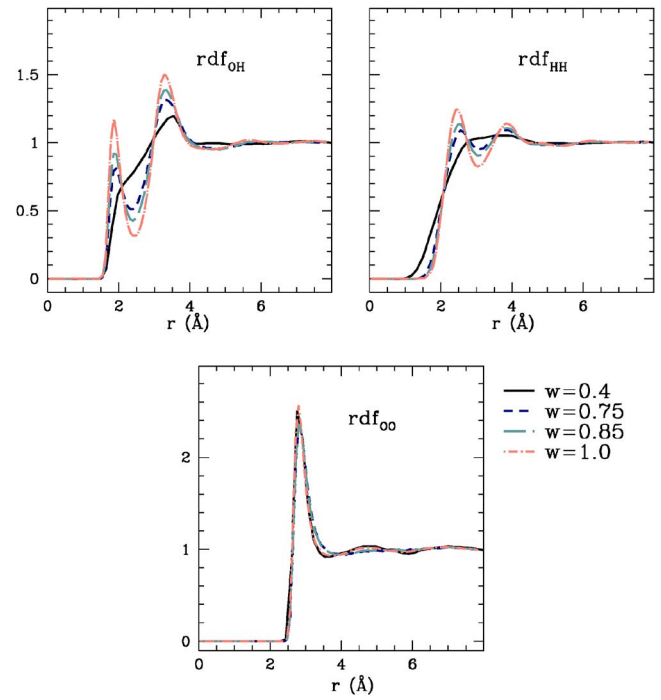

FIG. 10. (Color online) The H-H, O-H, and O-O rdf's for different particles identities. The water molecules start to correct their structural properties when $w > 0.6$.

molecular-based cutoff radius $R_c = 9$ Å are treated as a dielectric continuum with a dielectric constant $\epsilon_{RF} = 80$.[38,44–48] The Coulomb force acting on a partial charge e_{i_α}, belonging to the explicit or hybrid molecule α, at the center of the cutoff sphere, due to a partial charge e_{j_β}, belonging to the explicit or hybrid molecule β within the cavity, is

$$\mathbf{F}^{atom}_{C_{i_\alpha j_\beta}}(\mathbf{r}_{i_\alpha j_\beta}) = \frac{e_{i_\alpha} e_{j_\beta}}{4\pi\epsilon_0}\left[\frac{1}{r^3_{i_\alpha j_\beta}} - \frac{1}{R_c^3}\frac{2(\epsilon_{RF}-1)}{1+2\epsilon_{RF}}\right]\mathbf{r}_{i_\alpha j_\beta}. \quad (12)$$

To suppress the unphysical pressure fluctuations emerging as artifacts of the scheme given in Eq. (11), we employ an interface pressure correction[16] within the transition zone. The latter requires a reparametrization of the effective potential in the system composed of exclusively hybrid molecules (with a constant of $w = 1/2$). We redefine the center-of-mass intermolecular forces as

$$\mathbf{F}^{cm}_{\alpha\beta} = s[w(X_\alpha)w(X_\beta)]\mathbf{F}^{cm}_{\alpha\beta_o} + (1 - s[w(X_\alpha)w(X_\beta)])\mathbf{F}^{cm}_{\alpha\beta_{ic}}, \quad (13)$$

where the function $s \in [0,1]$ is defined as

$$s[x] = \begin{cases} \cos(\pi\sqrt{x})^2 & \text{if } 0 \le x < 0.25 \\ 4\left(\sqrt{x} - \frac{1}{2}\right)^2 & \text{if } 0.25 \le x \le 1.0 \end{cases}, \quad (14)$$

so the $s[0] = 1$, $s[1] = 1$, and $s[1/4] = 0$, as shown in Fig. 6. The interface correction force $F^{cm}_{\alpha\beta_{ic}}$ is the effective pair force between molecules α and β defined by the effective pair potential U^{cm}_{ic}, which is obtained by mapping the system composed of exclusively hybrid molecules with $w = 1/2$ to the explicit model system. The corrected effective potential

U^{cm}_{ic} shown in Fig. 5 is obtained by mapping the ex−cg ($w = 1/2$) system containing only hybrid molecules. The minima of the effective potential U^{cm}_{ic} become deeper, and a higher barrier separates the first and second hydration shell when compared to the center-of-mass effective potential U^{cm}. The center-of-mass rdf of the hydrid system exactly reproduces the structure of the references system as shown in Fig. 5.

The mixing function in Eq. (14) can correctly reproduce the thermodynamic properties of the hybrid atomistic/coarse-grained system with the same mean temperature (0.1% of difference) and pressure (0.5% of difference). Detailed comparisons between the bulk explicit simulations and the explicit regime in our hybrid setup prove that this approach does not alter the structural properties of the water model studied. In particular, Fig. 7 shows that the structural properties of the explicit regime in the multiscale system are exactly the same as in bulk explicit simulations. No change is detected in the orientational preferences of water molecules near the interface region. It is worth mentioning that similar results are obtained in the interface region (results not shown).

Figure 8 shows the probability density function of the orientational parameters $\cos\theta_{OH}$ (O-H vector and the normal of the interface surface) and $\cos\gamma_{HH}$ (H-H vector and the normal of the interface surface) in three consecutive layers of width 4 Å next to the interface region along the X-axis (see Fig. 1 for the definition of the regions). The uniform cosine distribution of the water molecules in layers inside and next to the interface indicates that the orientational DOFs are fully equilibrated in the hybrid region, as the molecules do not have to reorient upon crossing the interface region and there is no change of behavior at the interface.[17]
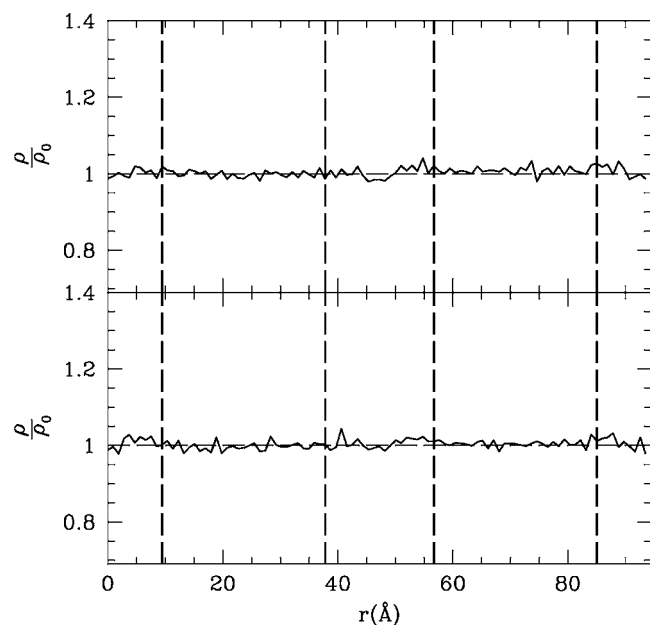
FIG. 11. Top figure: Normalized density profile in the *x*-direction of the mixed system when the position-dependent thermostat is used. Bottom figure: Normalized density profile in the *x*-direction of the mixed system when a constant friction constant is used.
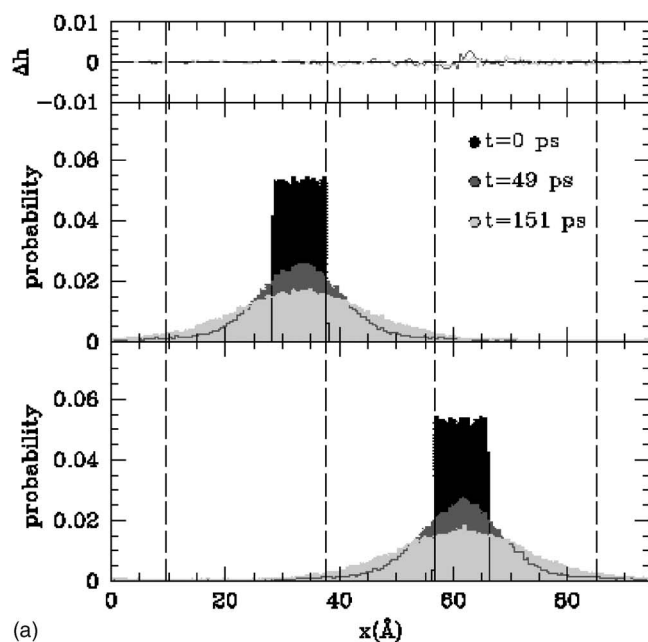
VI. POSITION-DEPENDENT THERMOSTAT

As mentioned above, the structural/thermodynamics of the coarse-grained system are not changed by increasing the background friction in the Langevin thermostat. To obtain the same diffusional dynamics across different resolutions, the coefficient Γ in the Langevin thermostat is changed on-the-fly depending on the number of DOFs of the molecules. As shown in Fig. 9, when a constant coefficient Γ is used, two regimes are observed in systems composed of only hybrid molecules:

- For $w \,\epsilon\, [0-0.6]$ the value of the diffusion coefficient D is essentially constant;

- For $w \,\epsilon\, [0.6-1.0]$ the value of the diffusion coefficient D drops steeply with w.

When the molecular identity w is greater than 0.6 the hybrid molecules start to equilibrate their orientational structure and their diffusive dynamics is slowed down, as shown in Figs. 9 and 10. In order to obtain the same diffusive dynamics for different levels of resolution, we propose the following functional form for the friction coefficient in the Langevin thermostat:

$$\Gamma(w) = \begin{cases} \Gamma_{cg} & \text{if } w \leq 0.6 \\ \alpha w + \beta & \text{if } 0.6 < w \leq 1.0 \end{cases}. \quad (15)$$

This choice provides a simple interpolation between the two limit values of $\Gamma(0.6) = \Gamma(0) = \Gamma_{cg} = 15$ ps^{-1} and $\Gamma(1) = \Gamma_{\text{all-atom}} = 5$ ps^{-1}. The parameters α and β are -25 and 30 ps^{-1}, respectively. As shown in Fig. 9, systems containing only hybrid molecules with different particle identities
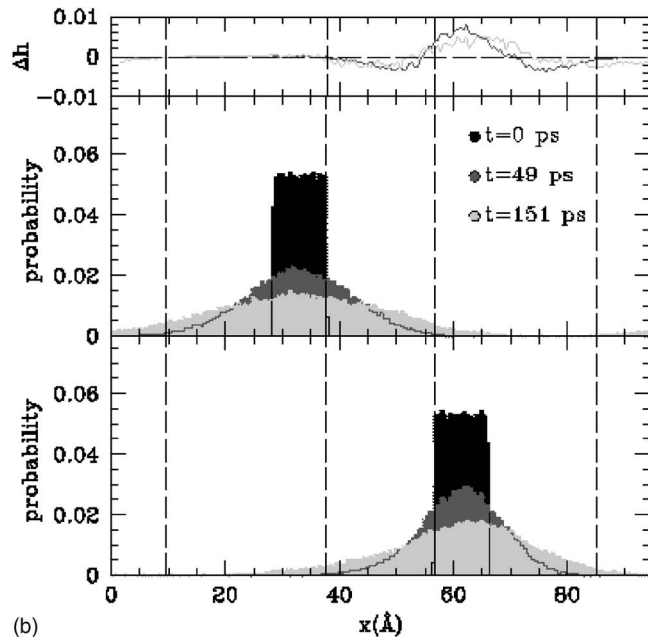
FIG. 12. (a) Time evolution of a diffusion profile when the position-dependent thermostat is used for molecules that are initially (at time $t = 0$ ps) located inside two neighboring slabs at opposite sides of the mid-interface layer. The diffusion profile is averaged over ≈ 400 different time origins. Vertical lines denote the boundaries of the interface layer. Bottom figure: The diffusion profile for the all-atom side is averaged over ≈ 400 different time origins. Middle figure: The same as before but for molecules that are initially localized inside the slab on the coarse-grained side of the interface region. Top figure: Difference between the corresponding diffusion profile of the coarse-grained and the all-atom regions. (b) Time evolution of a diffusion profile with the regular thermostat using the same criteria as given in (a).

exhibit the same diffusional dynamics when $\Gamma(w)$ has the functional form proposed in Eq. (15).

In our simulation we employ a local Langevin thermostat with a position-dependent friction[49–52] to match the diffusion constants of the coarse-grained and all-atom regimes. The Langevin equation with a position dependent coefficient $\Gamma(x)$ can be written as[49]
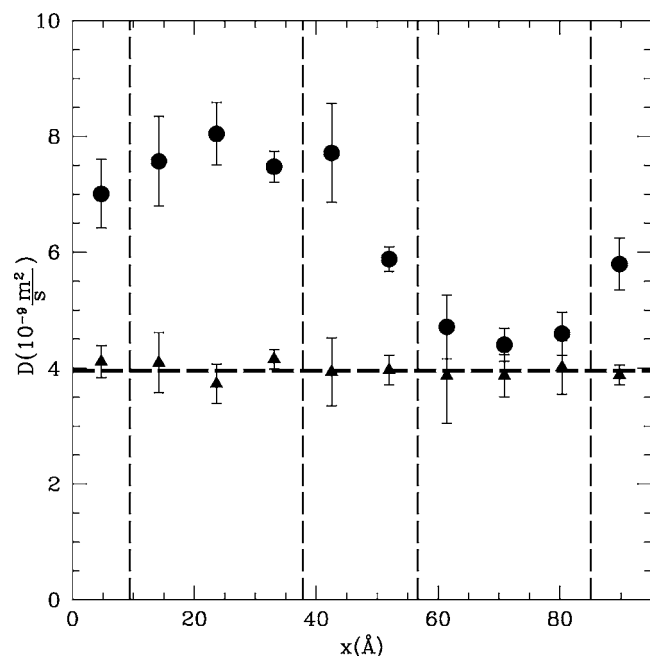
FIG. 13. Diffusion coefficient as a function of the x position using particles that are within a slab of ≈ 9.5 Å of the hybrid system for different type of thermostats. Each point in the plot is centered in each slab. The average is over ≈ 400 different time origins. The horizontal line is the diffusion coefficient of a system containing only all-atom water molecules. The dots indicate the diffusion of the molecules across the hybrid system when the regular thermostat is used. The triangles indicate the diffusion of the molecules across the hybrid system when the position-dependent thermostat is used.

$$m_i dv_i/dt = F_i - m_i \Gamma(x) v_i + R_i(x,t), \quad (16)$$

where $R_i(x,t)$ is

$$\langle R_i(x,t) \rangle = 0, \quad (17)$$

$$\langle R_i(x,t_1) R_j(x,t_2) \rangle = 2\Gamma(x) m_i kT \delta(t_1 - t_2) \delta_{ij}. \quad (18)$$

The functional form of $\Gamma(x)$ depends on the weighting function $w(x)$ and it is shown in Fig. 9 [see Eq. (15)]. There is no difference in the structural and thermodynamic properties of the system when a position-dependent $\Gamma(x)$ is used instead of a constant coefficient Γ. The density is homogeneous in both the coarse-grained and explicit regions with (very) small oscillations in the transition regime; cf. Fig. 11.

To prove the free exchange of molecules between the different regimes, we have computed the time evolution of a diffusion profile for molecules that were initially localized within two slabs of width ≈ 9.5 Å neighboring the interface layer. The molecules initially localized within the two slabs spread out symmetrically with time when a position-dependent friction is used in the local thermostat. On the contrary, the molecules spread out asymmetrically with time as shown in Fig. 12 when a fixed coefficient Γ is used. This asymmetry arises from the above-mentioned difference in diffusion coefficient D between the all-atom and coarse-grained regions (see Ref. 17). Figure 13 shows the behavior of the diffusion coefficient D as a function of the x position using particles that are within a slab of ≈ 9.5 Å of the mixed system for the two different types of thermostats. As Fig. 13 illustrates, the molecules are slowed down when they cross

the interface from the coarse-grained region to the explicit region if a constant friction is used for the thermostat. The change in the diffusion coefficient D is localized in the interface region while D is approximately constant inside each region, coarse-grained $[D \approx (8.04 \pm 0.54) \times 10^{-9}$ m^2/s] and explicit $[D \approx (4.2 \pm 0.28) \times 10^{-9}$ m^2/s]. When a position-dependent friction is used for the local thermostat, the diffusive dynamics of the molecules is the same as for the all-atom system across all regions, as shown in Fig. 13.

VII. CONCLUSIONS

In this paper we extended the multiscale model for water that we have recently proposed[17] to obtain the same diffusional dynamics across the different resolutions. We also studied the accuracy of different coarse-grained water models in reproducing the structural properties of the all-atom system. The results of this study show that for our purposes the single-site model performs equally well as the more sophisticated (three-site and two-site) coarse-grained models and is hence the most appropriate for the presented adaptive resolution simulations. We envisage that such adaptive resolution simulations of water will play an important role in the modeling of biomolecular systems where the coupling of different time and length scales is crucial to understand their physico-chemical properties.

APPENDIX: COMPUTATIONAL DETAILS

1. Multiscale simulation protocol

All the results presented in the paper were obtained by performing *NVT* simulations using the ESPRESSO (Ref. 53) (for the one-site and multiscale model) and AMBER 8 (Ref. 54) (for the two-site and three-site models) simulation packages with a Langevin thermostat, with a friction constant Γ =5 ps^{-1} when a regular thermostat is used and a time step of 0.002 ps. All the models considered a system of 1464 water molecules at T_{ref}=300 K and ρ=0.96 g/cm^3. The density was obtained from an all-atom *NPT* simulation with P_{ref} =1 atm using a reaction-field method for the electrostatics and a cutoff method for the pressure. The results presented for the two-site and three-site models were obtained for a density ρ=1.007 g/cm^3. This value of the density was obtained from an all-atom *NPT* simulation with P_{ref}=1 atm using a Ewald method for the electrostatics and a long-ranged correction for the pressure after the cutoff. Periodic boundary conditions and minimum image convention were applied in all directions. The bonds and angle of the water molecules were constrained by using the RATTLE procedure.[55] After warm-up and equilibration, several trajec-
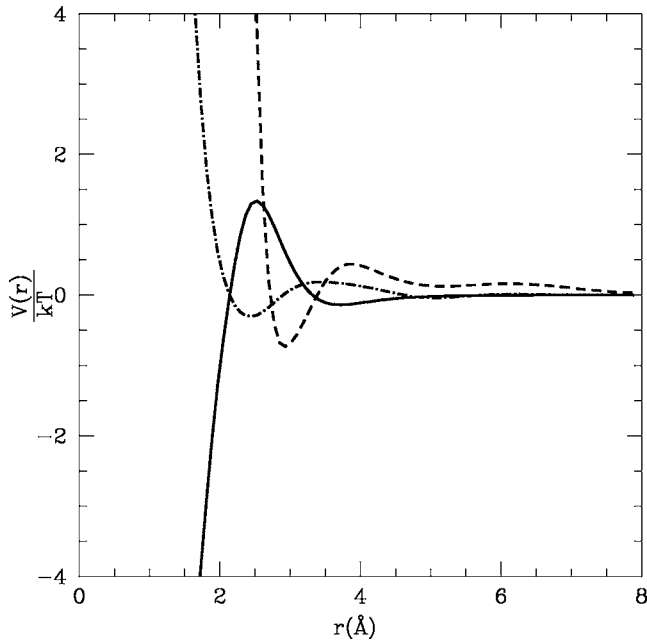
FIG. 14. Effective pair potentials for the three-site water model. The dashed, dashed-dot, and full line curves indicate the O-O, H-H, and O-H interactions, respectively.

tories of 1.5 ns each were collected for each different model. All simulations were performed with a force capping to prevent possible force singularities that could emerge because of overlaps with neighboring molecules when a given molecule enters the interface layer from the coarse-grained side. The size of the system is 94.5 Å in the x direction and 22 Å in both the y and z directions. An interface layer of 18.9 Å between the coarse-grained and all-atom models is set along the x direction. To treat all the molecules of the system equally, regardless of their level of detail, we define the pres-
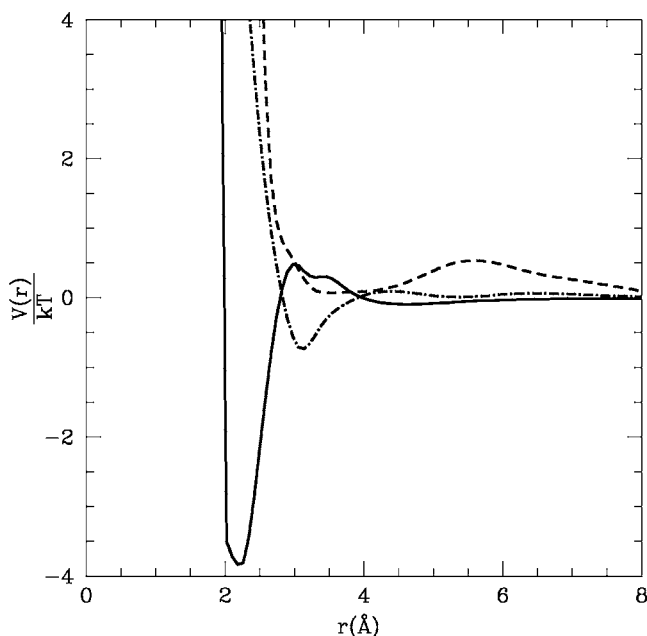

FIG. 15. Effective pair potentials for the two-site water model. The dashed, dashed-dot, and full line curves indicate the O-O, dipole-dipole, and O-dipole interactions, respectively.

sure of the system according to their lower level of detail, that is by the molecular pressure.[15,16,56,57] The temperature was evaluated using the fractional analog of the equipartition theorem,

$$\langle K_\alpha \rangle = \frac{\alpha k_B T}{2},\tag{A1}$$

where $\langle K_\alpha \rangle$ is the average kinetic energy per fractional quadratic DOF with the weight $w(r) = \alpha$.[13] Via Eq. (A1) the temperature is also rigorously defined in the transition regime in which the rotational DOFs are partially "switched on/off."

For each of the models considered, the following expression:

$$\frac{V(r)}{kT} = a_0\left[\left(\frac{r_0}{r}\right)^\alpha - \left(\frac{r_0}{r}\right)^\beta\right] + a_1 e^{-b_1(r-r_1)^2}$$
$$+ a_2 e^{-b_2(r-r_2)^2} + a_3 e^{-b_3(r-r_3)^2} + a_4 e^{-b_4(r-r_4)^2}$$
$$+ a_5 e^{-b_5(r-r_5)^2},\tag{A2}$$

is fitted within line thickness to the tabulated effective potential.

2. Three-site interaction model

The coarse-graining procedure described in the paper converges after 12 iterations, yielding the effective potentials shown in Fig. 14. The parameters of the effective potential [Eq. (A2)] obtained for the three-site model are listed below.

	α	β	a_0	a_1	a_2	a_3	a_4	a_5
O-O	25.8	21.35	130.3	10.8	−1.23	−10.6	53.0	0.0
O-H	13.48	6.96	214.8	−19.2	73.9	−32.25	7.53	0.0
H-H	29.87	23.24	15.9	−0.57	−0.11	49.45	0.23	0.0

(Å)	r_0	r_1	r_2	r_3	r_4	r_5
O-O	2.3	4.3	2.9	4.34	2.02	0.0
O-H	1.28	−0.77	1.41	1.53	1.88	0.0
H-H	1.27	2.38	4.88	0.56	2.62	0.0

(Å⁻¹)	b_1	b_2	b_3	b_4	b_5
O-O	0.35	3.53	0.38	6.6	0.0
O-H	0.25	7.0	10.47	1.25	0.0
H-H	3.45	1.88	2.12	0.22	0.0

3. Two-site interaction model

The coarse-graining procedure converges after 25 iterations; the resulting effective potential is shown in Fig. 15. The parameters of the effective potential are listed below.

	α	β	a_0	a_1	a_2	a_3	a_4	a_5
O-O	23.8	21.5	239.0	9.0	0.81	−12.75	69.6	0.0
O-d	20.1	7.5	157.4	−7.5	82.0	−71.0	−0.3	28.7
d-d	41.5	4.9	−19.3	0.38	−0.17	45.7	0.91	0.0

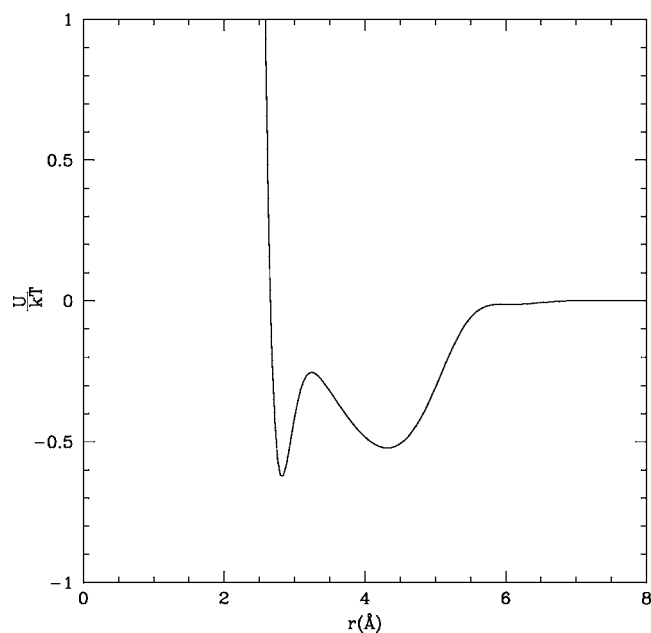| (Å)	r_0	r_1	r_2	r_3	r_4	r_5
O-O	2.31	5.44	2.9	5.41	1.92	0.0

FIG. 16. The effective interaction between the center-of-mass of two molecules as obtained for the single-site water model.

(Å)	r_0	r_1	r_2	r_3	r_4	r_5
O-d	1.89	2.4	1.6	1.8	3.2	1.7
d-d	1.93	3.1	5.2	1.23	1.86	0.0

(Å^{-1})	b_1	b_2	b_3	b_4	b_5
O-O	0.48	12.5	0.56	5.03	0.0
O-d	0.8	3.6	32.0	20.6	0.55
d-d	15.52	1.2	1.2	0.09	0.0

4. One-site interaction model

The coarse-graining procedure converges after 8 iterations. The resulting potential for the effective interaction between the center-of-mass of two molecules is shown in Fig. 16; the parameters obtained from the fit to Eq. (A2) are listed below.

	α	β	a_0	a_1	a_2	a_3	a_4	a_5
cm-cm	16.47	16.29	0.13	0.15	0.42	−0.93	−1.37	0.0

(Å)	r_0	r_1	r_2	r_3	r_4	r_5
cm-cm	3.66	5.43	4.5	4.4	2.62	0.0

(Å^{-1})	b_1	b_2	b_3	b_4	b_5
cm-cm	3.0	0.47	0.59	8.6	0.0

[1] S. Pal, J. Peon, and A. Zewail, Proc. Natl. Acad. Sci. U.S.A. **99**, 15297 (2002).
[2] M. Cheung, A. Garcia, and J. Onuchic, Proc. Natl. Acad. Sci. U.S.A. **99**, 685 (2002).
[3] M. Praprotnik and D. Janežič, J. Chem. Phys. **122**, 174103 (2005).
[4] J. Q. Broughton, F. F. Abraham, N. Bernstein, and E. Kaxiras, Phys. Rev. B **60**, 2391 (1999).
[5] G. Csanyi, T. Albaret, M. C. Payne, and A. DeVita, Phys. Rev. Lett. **93**, 175503 (2004).
[6] K. Kremer, in *Multiscale Modelling and Simulation*, Lecture Notes on Computational Science and Engineering, edited by S. Attinger and P. Koumoutsakis (Springer, Berlin, 2004).
[7] P. Koumoutsakos, Annu. Rev. Fluid Mech. **37**, 457 (2005).
[8] M. Neri, C. Anselmi, M. Cascella, A. Maritan, and P. Carloni, Phys. Rev. Lett. **95**, 218102 (2005).
[9] J. A. Backer, C. P. Lowe, and H. C. J. Ledema, J. Chem. Phys. **123**, 114905 (2005).
[10] C. F. Abrams, J. Chem. Phys. **123**, 234101 (2005).
[11] G. De Fabritiis, R. Delgado-Buscalioni, and P. V. Coveney, Phys. Rev. Lett. **97**, 134501 (2006).
[12] E. Lyman, F. M. Ytreberg, and D. M. Zuckerman, Phys. Rev. Lett. **96**, 028105 (2006).
[13] M. Praprotnik, K. Kremer, and L. Delle Site, Phys. Rev. E **75**, 017701 (2007).
[14] M. Praprotnik, K. Kremer, and L. Delle Site, J. Phys. A **40**, F281 (2007).
[15] M. Praprotnik, L. Delle Site, and K. Kremer, J. Chem. Phys. **123**, 224106 (2005).
[16] M. Praprotnik, L. Delle Site, and K. Kremer, Phys. Rev. E **73**, 066701 (2006).
[17] M. Praprotnik, S. Matysiak, L. Delle Site, K. Kremer, and C. Clementi, J. Phys.: Condens. Matter **19**, 292201 (2007).
[18] S. Matysiak, A. Montesi, A. B. Kolomeisky, M. Pasquali, and C. Clementi, Phys. Rev. Lett. **96**, 118103 (2006).
[19] W. L. Jorgensen, J. Chandrasekhar, J. D. Madura, R. W. Impey, and M. L. Klein, J. Chem. Phys. **79**, 926 (1983).
[20] A. P. Lyubartsev and A. Laaksonen, Phys. Rev. E **52**, 3730 (1995).
[21] S. Matysiak and C. Clementi, J. Mol. Biol. **343**, 235 (2004).
[22] S. Matysiak and C. Clementi, J. Mol. Biol. **363**, 297 (2006).
[23] D. Reith, M. Putz, and F. Müller-Plathe, J. Comput. Chem. **24**, 1624 (2003).
[24] K. A. Dill, T. M. Truskett, V. Vlachy, and B. Hribar-Lee, Annu. Rev. Biophys. Biomol. Struct. **34**, 173 (2005).
[25] S. Garde and H. S. Ashbaugh, J. Chem. Phys. **115**, 977 (2001).
[26] S. Izvekov and G. A. Voth, J. Chem. Phys. **123**, 134105 (2005).
[27] T. Head-Gordon and F. H. Stillinger, J. Chem. Phys. **98**, 3313 (1993).
[28] A. K. Soper, Chem. Phys. **202**, 295 (1996).
[29] I. Nezbeda, Mol. Phys. **103**, 59 (2005).
[30] S. J. Marrink, A. H. de Vries, and A. E. Mark, J. Phys. Chem. B **108**, 750 (2004).
[31] J. C. Shelley, M. Y. Shelley, R. C. Reeder, S. Bandyopadhyay, and M. L. Klein, J. Phys. Chem. B **105**, 4464 (2001).
[32] A. P. Lyubartsev and A. Laaksonen, Chem. Phys. Lett. **325**, 15 (2000).
[33] J. R. Errington and P. G. Debenedetti, Nature (London) **409**, 318 (2001).
[34] M. E. Johnson, T. Head-Gordon, and A. A. Louis, J. Chem. Phys. **126**, 144509 (2007).
[35] W. Tschöp, K. Kremer, J. Batoulis, T. Bürger, and O. Hahn, Acta Polym. **49**, 61 (1998).
[36] S. Izvekov and G. A. Voth, J. Chem. Phys. **125**, 151101 (2006).
[37] K. Kremer and G. S. Grest, J. Chem. Phys. **92**, 5057 (1990).
[38] I. G. Tironi, R. Sperb, P. E. Smith, and W. F. van Gunsteren, J. Chem. Phys. **102**, 5451 (1995).
[39] T. Soddemann, B. Dünweg, and K. Kremer, Phys. Rev. E **68**, 046702 (2003).
[40] M. Praprotnik, L. Delle Site, and K. Kremer, J. Chem. Phys. **126**, 134902 (2007).
[41] H. Goldstein, *Classical Mechanics*, 2nd ed. (Addison-Wesley, Reading, MA, 1980).
[42] L. Delle Site, Phys. Rev. E **76**, 047701 (2007).
[43] B. Ensing, S. O. Nielsen, P. B. Moore, M. L. Klein, and M. Parrinello, J. Chem. Theory Comput. **3**, 1100 (2007).
[44] M. Neumann, Mol. Phys. **50**, 841 (1983).
[45] M. Neumann, J. Chem. Phys. **82**, 5663 (1985).
[46] M. Neumann, J. Chem. Phys. **85**, 1567 (1986).
[47] W. Im, S. Berneche, and B. Roux, J. Chem. Phys. **114**, 2924 (2001).
[48] M. Praprotnik, D. Janežič, and J. Mavri, J. Phys. Chem. A **108**, 11056 (2004).
[49] B. Carmeli and A. Nitzan, Chem. Phys. Lett. **102**, 517 (1983).
[50] M. J. Moix and R. Hernandez, J. Chem. Phys. **122**, 114111 (2005).
[51] P. Grigolini, J. Chem. Phys. **89**, 4300 (1988).
[52] J. B. Straus and G. A. Voth, J. Chem. Phys. **96**, 5460 (1992).
[53] H. J. Limbach, A. Arnold, B. A. Mann, and C. Holm, Comput. Phys.

Commun. **174**, 704 (2006); http://www.espresso.mpg.de

[54] D. A. Pearlman, D. A. Case, J. W. Caldwell, W. S. Ross, T. E. Cheatam, D. M. Ferguson, U. Chandra Singh, P. Weiner, and P. A. Kollman, AMBER, Ver. 4.1 (1995).

[55] H. C. Andersen, J. Comput. Phys. **52**, 24 (1983).

[56] H. Berendsen, J. Postma, W. V. Gunsteren, A. D. Nola, and J. Haak, J. Chem. Phys. **81**, 3684 (1984).

[57] R. L. C. Akkermans and G. Ciccotti, J. Phys. Chem. B **108**, 6866 (2004).